Assessment of WENO and TENO schemes for the four-equation compressible two-phase flow model with regularization terms

By H. Collis, S. Mirjalili, S. S. Jain, AND A. Mani

1. Motivation and objectives

Development of essentially non-oscillatory (ENO) discretization schemes began in the 1980s with works including Harten *et al.* (1987) and Shu & Osher (1988, 1989), and had a breakthrough in popularity with the development of weighted-ENO (WENO) scheme (Liu 1994; Jiang & Shu 1996). Recently, the targeted-ENO (TENO) scheme was developed as an improvement to traditional WENO schemes by producing less numerical dissipation (Fu *et al.* 2016). The ability of ENO-type schemes to capture discontinuities makes them popular for complex multi-physics problems that involve shocks, contact discontinuities, material interfaces, and even flame fronts. However, ENO-type schemes have significant shortcomings when they are used for resolving material interfaces: these schemes will continually diffuse material interfaces throughout time and do not satisfy the boundedness criteria of the volume fraction of phases. Both of these issues can lead to large errors when they occur in a multi-physics code. Many works propose interface regularization terms that prevent continual diffusion, but they are generally written in non-conservative form (Shukla *et al.* 2010; Tiwari *et al.* 2013). Chiu & Lin (2011) developed interface regularization terms in conservative form—a conservative diffuse-interface method (CDI)—for incompressible flows. More recently, Jain *et al.* (2020) extended the CDI formulation to compressible flows and further improved their accuracy using the accurate CDI (ACDI) formulation (Jain 2022). Additionally, Mirjalili *et al.* (2020) and Jain *et al.* (2020) demonstrated that volume fraction boundedness can be achieved with CDI [and ACDI (Jain 2022)] regularization terms using second-order centered-differences for incompressible and compressible flows, respectively. However, unlike ENO-type schemes, centered-difference schemes are not appropriate for complex problems involving shocks and other flow discontinuities unless augmented by additional regularization [eg. LAD schemes (Cook 2007; Kawai & Lele 2008; Mani *et al.* 2009; Mirjalili *et al.* 2021; Jain & Moin 2021)]. The objective of this work is to outline the issues of using ENO-type schemes in four-equation models for compressible two-phase flow simulations and illustrate how coupling ENO-type schemes with the ACDI interface regularization terms leads to improved two-phase flow simulations.

2. Numerical framework

2.1. *Governing equations*

This work uses the four-equation model, which is derived from the general seven-equation model of Baer & Nunziato (1986) by assuming a single equilibrium pressure, tempera-

ture, and velocity field between the two phases (Saurel & Pantano 2018). The system of equations is shown in Eqs. (2.1)–(2.3).

$$\frac{\partial m_l}{\partial t} + \vec{\nabla} \cdot (\vec{u} m_l) = 0, \quad l = 1, 2 \tag{2.1}$$

$$\frac{\partial \rho \vec{u}}{\partial t} + \vec{\nabla} \cdot (\rho \vec{u} \otimes \vec{u} + P\mathbb{1}) = \vec{\nabla} \cdot \tau + \vec{F}_{ST} + \rho \vec{g} \tag{2.2}$$

$$\frac{\partial E}{\partial t} + \vec{\nabla} \cdot (\vec{u} E) + \vec{\nabla} \cdot (P\vec{u}) = \vec{\nabla} \cdot (\tau \cdot \vec{u}) + \vec{\nabla} \cdot (\lambda \nabla T) + \vec{u} \cdot F_{ST} + \rho \vec{g} \cdot \vec{u} \tag{2.3}$$

Here, m_l is the mass per unit volume of phase l, ρ is the mixture density and can be given by $\rho = \sum_l m_l$, $\vec{u}$ is the velocity, E is the total energy per unit volume, T is the temperature, P is the pressure, λ is the thermal conductivity and $\vec{g}$ is a body force due to gravity. Furthermore, problems with surface tension include $\vec{F}_{ST}$ (the surface-tension force). In this work, both the surface tension and thermal conductivity are set to zero. The viscous stress tensor, τ is given by,

$$\tau = \mu[\nabla \vec{u} + \nabla \vec{u}^T - 2(\vec{\nabla} \cdot \vec{u})\mathbb{1}/3], \tag{2.4}$$

where μ is the dynamic viscosity. Lastly, this work uses the stiffened-gas equation of state

$$P(\rho, e) = (\gamma - 1)\rho e - \gamma P_0, \tag{2.5}$$

where e is the internal energy per unit volume, γ is the polytropic coefficient, and P_0 is the reference pressure.

As mentioned above, the four-equation model enforces both mechanical and thermal equilibrium of phases within the same computational cell. To enforce these conditions this work uses an iterative procedure developed by Flåtten *et al.* (2011) for the stiffened-gas equation of state that provides the pressure, temperature, and volume fraction needed for mechanical and thermal equilibrium.

2.2. *ENO-type scheme formulations*

ENO-type schemes are designed to sense oscillations in the field variables and at those locations use a combination of upwinding schemes to give "essentially non-oscillatory" solutions. These schemes have been proven to work well for many flows with discontinuities (Pirozzoli 2011; San & Kara 2014; Fu 2019; Di Renzo *et al.* 2020). In Eqs. (2.1)–(2.3), the Euler fluxes are nonlinear and responsible for the formation of discontinuities. So, ENO-like discretization is generally applied only to the Euler fluxes, and the viscous flux terms are discretized using centered-differences. This is the methodology that is followed in this work as well.

When formulating ENO-type schemes in a finite-difference setting, single-phase multicomponent simulations have improved efficiency and accuracy using the conservative variables for the ENO-like flux reconstruction (Fu *et al.* 2016; Di Renzo *et al.* 2020). However, unlike other discontinuities, material interfaces require that the velocity and pressure through the interface stay constant. This property is called the interface equilibrium condition (IEC) and to avoid numerically induced oscillations around interfaces, the IEC must be discretely satisfied. Five-equation models can be carefully discretized to satisfy the IEC for both centered-difference schemes and ENO-like formulations (Johnsen & Colonius 2006; Jain & Moin 2022). For ENO-type schemes, the IEC is satisfied only if the ENO-like reconstruction is done using primitive variables (Johnsen & Colonius 2006;

Johnsen & Ham 2012; Movahed & Johnsen 2013; Coralic & Colonius 2014). However, since the four-equation model uses an iterative procedure to find the pressure, it is practically impossible to discretely satisfy the IEC. Thus, motivated by the benefits seen in single-phase multicomponent flows, this work uses the conservative variables in the flux reconstruction for WENO and TENO.

To avoid oscillations across other discontinuities, the flux reconstruction for the ENO-type schemes is performed in characteristic space. Details of this formulation, including examples of the eigenvalues and eigenvectors, are included in Di Renzo *et al.* (2020). The main differences in this work, compared to Di Renzo *et al.* (2020), are the definitions of the pressure derivatives needed for the characteristic projection. Particularly, the pressure derivatives must be derived to incorporate the assumptions of the four-equation model (thermal and mechanical equilibrium) along with the stiffened-gas equation of state. These assumptions can be enforced by solving a linear system of equations, but for brevity, the derivation is not included here. The pressure derivatives and the equation for the speed of sound are shown in Eqs. (2.6)–(2.10). The speed of sound is given by

$$c^2 = \frac{1}{\rho}\left(H - \frac{E}{\rho}\right)\left(\frac{\partial P}{\partial e}\right)_{m_1,m_2} + Y_1\left(\frac{\partial P}{\partial m_1}\right)_{e,m_2} + Y_2\left(\frac{\partial P}{\partial m_2}\right)_{e,m_1}, \tag{2.6}$$

where $H = (E+P)/\rho$ is the total enthalpy and $Y_i = m_i/(\sum_l m_l)$ are the mass fractions of phase i. Equation (2.7) shows the form of the exact differential found by solving the system of equations described above.

$$dP = A(Bde + Cdm_1 + Ddm_2) \tag{2.7}$$

With the pressure differential, the pressure derivatives can be found using

$$\left(\frac{\partial P}{\partial e}\right)_{m_1,m_2} = A * B, \quad \left(\frac{\partial P}{\partial m_1}\right)_{e,m_2} = A * C, \quad \text{and} \quad \left(\frac{\partial P}{\partial m_2}\right)_{e,m_1} = A * D. \tag{2.8}$$

The definition for these variables assuming the stiffened-gas equation of state is given by

$$A = \frac{(P + P_{0_1})(P + P_{0_2})}{\left(\phi_1 \frac{P+P_{0_1}}{\gamma_1 - 1} + \phi_2 \frac{P+P_{0_2}}{\gamma_2 - 1}\right)\left[\phi_2(P + P_{0_1}) + \phi_1(P + P_{0_2})\right] + \phi_1\phi_2(P_{0_1} - P_{0_2})^2} \tag{2.9}$$

$$B = \rho, \quad C = \phi_1 e_1 + \frac{e_2\phi_2\rho_2}{\rho_1} - e_1 + e, \text{ and } \quad D = \phi_2 e_2 + \frac{e_1\phi_1\rho_1}{\rho_2} - e_2 + e. \tag{2.10}$$

The summation of pressure derivatives in Eq. (2.6) is always positive (for positive mass fraction), which guarantees a positive speed of sound. After the pressure derivatives have been found, the reconstruction can be completed using the algorithm illustrated by Di Renzo *et al.* (2020). In this work, the ENO-type schemes used are the original WENO5-JS (Jiang & Shu 1996) and TENO6 (Fu *et al.* 2016).

2.3. *Interface regularization*

Another methodology for simulating two-phase flows with diffuse interfaces is adding specifically designed interface regularization terms to the governing equations. Many interface regularization terms have been developed for this purpose (Cook 2007; Shukla *et al.* 2010; Tiwari *et al.* 2013; Subramaniam *et al.* 2018; Jain *et al.* 2020). This work has chosen to use the ACDI terms developed by Jain (2022), which are written in fully conservative form to achieve discrete conservation. Using the ACDI formulation has been

shown to guarantee creation of material interfaces with a thickness that remains finite, resolvable, and numerically constant (Jain *et al.* 2020; Jain 2022). Furthermore, the ACDI terms provide strictly bounded volume fractions (when using second-order centered-differences). The new governing equations (assuming no surface tension or heat transfer) with the ACDI terms added are shown below.

$$\frac{\partial m_l}{\partial t} + \vec{\nabla} \cdot (\vec{u} m_l) = \vec{\nabla} \cdot \vec{R}_l, \quad l = 1, 2 \tag{2.11}$$

$$\frac{\partial \rho \vec{u}}{\partial t} + \vec{\nabla} \cdot (\rho \vec{u} \otimes \vec{u} + P\mathbb{1}) = \vec{\nabla} \cdot \tau + \rho \vec{g} + \vec{\nabla} \cdot (\vec{f} \otimes \vec{u}) \tag{2.12}$$

$$\frac{\partial E}{\partial t} + \vec{\nabla} \cdot (\vec{u} E) + \vec{\nabla} \cdot (P\vec{u}) = \vec{\nabla} \cdot (\tau \cdot \vec{u}) + \rho \vec{g} \cdot \vec{u} + \vec{\nabla} \cdot (\vec{f} k) + \sum_l \vec{\nabla} \cdot (\rho_l h_l \vec{a}_l) \tag{2.13}$$

In Eqs. (2.11)-(2.13), $h_l = e_l + P/\rho_l$ is the enthalpy of phase l, $k = \sum_i^3 u_i^2/2$ is the kinetic energy, and the highlighted terms are defined using

$$\vec{R}_l = \rho_l \Gamma \left\{ \epsilon \vec{\nabla} \phi_l - \frac{1}{4} \left[1 - \tanh^2 \left(\frac{\psi}{2\epsilon} \right) \right] \frac{\vec{\nabla} \psi}{|\vec{\nabla} \psi|} \right\}, \qquad \vec{f} = \sum_{l=1}^{2} \vec{R}_l, \quad \text{and} \quad \vec{a_l} = \vec{R}_l / \rho_l,$$

where ψ is defined as

$$\epsilon \ln \left(\frac{\phi + \eta}{1 - \phi + \eta} \right),$$

with η being set to a small value ($\eta = 10^{-100}$ is used in this work). The system is closed by noting that $\vec{a_1} = -\vec{a_2}$ and taking $\Gamma = \max |\vec{u}|$ and $\epsilon > 0.5 \Delta x$.

In past works Eqs. (2.11)–(2.13) have been solved using low-dissipation schemes [centered/compact differences (Jain *et al.* 2020, 2021; Jain 2022)]. In these works the ACDI terms properly regulate material interfaces including for high density ratios and under large deformations. But, since these terms are designed just for material interfaces, they will not capture shocks or regularize contact discontinuities. This requires the user to add additional treatments, [eg. LAD methods of shocks (Cook & Cabot 2005; Kawai & Lele 2008; Mani *et al.* 2009; Jain & Moin 2021; Mirjalili *et al.* 2021)] which can require parameter tuning for acceptable results.

2.4. *Combining ENO-type schemes with ACDI terms*

There are trade-offs to both diffuse interface methodologies described above. The ENO-type schemes provide robustness for handling many discontinuities that occur in multi-physics problems, but they do not satisfy essential requirements for material interfaces. Combining interface regularization terms with ENO-type schemes can provide a simulation framework that satisfies three vital properties for simulations of compressible multiphase flows: 1) volume fractions boundedness, 2) discrete conservation, and 3) capturing of discontinuities.

2.4.1. *Volume fraction boundedness*

To be physically consistent, the volume fraction of both phases must sum to 1. If the volume fraction of a phase is over 1, or below 0, this is equivalent to filling/draining of those phases, respectively. To avoid this, some works will clip the volume fraction to strictly enforce that it stays bounded, but clipping is equivalent to removing mass.

Breaking boundedness is an important issue for all two-phase codes, but especially so for codes that also include complex multi-physics like chemical reactions and combustion. Current ENO-like formulations ignore this requirement and focus only on satisfaction of the IEC. As described in Section 2.3 the regularization terms have been designed to provide bounded volume fraction if the discretization scheme is second-order centered-difference. In this work, the ACDI terms are combined with WENO and TENO schemes to help satisfy the boundedness requirement.

2.4.2. *Conservation of mass, momentum, and energy*

In addition to keeping the volume fraction bounded, another vital requirement for discrete conservation is writing the governing equations in conservative form. Most past works using ENO-type schemes for compressible flows write at least one conservation equation in non-conservative form (Johnsen & Colonius 2006; Movahed & Johnsen 2013; Coralic & Colonius 2014; Wong *et al.* 2021). In this work, all terms in the governing equations, including the interface regularization terms, have been written in conservative form to ensure discrete conservation.

2.4.3. *Capturing discontinuities*

ENO-type schemes are excellent at capturing shocks, but they will continually diffuse material interfaces. Combining ENO-type schemes with the ACDI terms that sharpen material interfaces provides resolvable interface boundaries between immiscible phases.

2.4.4. *Numerical implementation*

In Eqs. (2.11)–(2.13), only the Euler fluxes are discretized using the high-order ENO-type schemes and all other terms (viscous and ACDI) are discretized using second-order centered-difference schemes. A third-order Runge–Kutta method is used for time integration for all test cases. The implementation was completed within the highly parallel hydrodynamics task-based research code: HTR (Di Renzo *et al.* 2020).

3. Results

Several computational experiments are used to assess the performance of ENO-type schemes with and without the ACDI terms. First, two shock tube test cases are presented to show that the schemes perform well with and without ACDI terms. Second, simulations of a Rayleigh–Taylor instability performed at low resolutions is used to assess the robustness of the ENO-type schemes for predicting interface deformations. Lastly, a shock-bubble interaction is presented to test the ability of the ENO-type schemes to handle simulations with both interface deformation and shock discontinuities. We note that all parameters and numbers in this section are dimensionless.

3.1. *Shock tube*

3.1.1. *Helium–air shock tube*

This problem involves a Mach 8.96 shock wave in Helium that travels into a material interface with air. Originally this problem was posed by Liu *et al.* (2003); later modified by Johnsen & Colonius (2009) and has been studied extensively. As reported by Coralic & Colonius (2014) it is a difficult problem for diffuse interface methods that sharpen the interface (like ACDI). It is also a verification test for discrete conservation, since if conservation is lost the position and speed of the shock-waves will be miscalculated. The

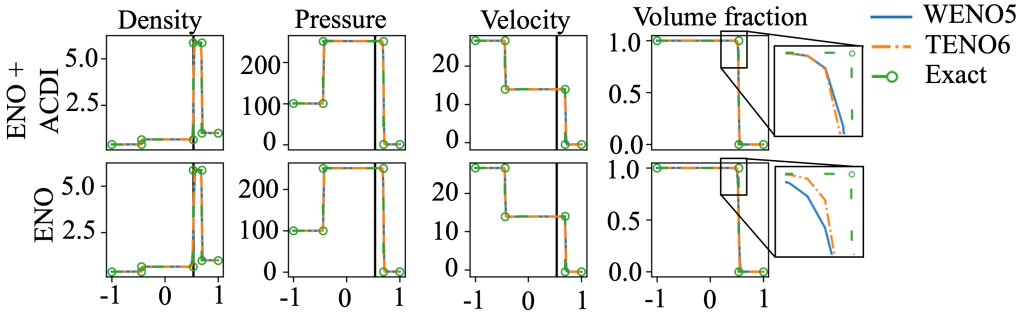

FIGURE 1. Plots of density, pressure, velocity, and volume fraction for the helium-air shock tube problem at t = 0.07. The material interface location is marked in other flow fields with a black line.

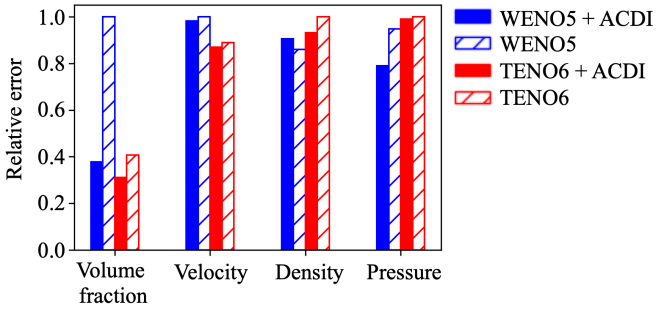

FIGURE 2. Relative error for volume fraction, velocity, density, and pressure fields for each discretization scheme used to solve the helium–air shock tube problem.

simulation setup is identical to that used by Coralic & Colonius (2014) with 200 grid points, Dirichlet boundary conditions, and an initial condition given by

$$(m_1, m_2, u, P, \phi_1) = \begin{cases} (0.386, 0.0, 26.59, 100.0, 1.0) & \text{if } -1 \le x < -0.8, \\ (0.1, 0.0, -0.50, 1.0, 1.0) & \text{if } -0.8 \le x < -0.2, \text{ and} \\ (0.0, 1.0, -0.50, 1.0, 0.0) & \text{if } -0.2 \le x \le 1.0. \end{cases} \quad (3.1)$$

In Figure 1, the exact profile is given as a reference for both ENO-type schemes with and without the ACDI terms. All schemes visually match the exact solution with accurate shock locations and no visual oscillations.

To quantitatively compare the performance of the different schemes, the relative error is plotted in Figure 2. WENO5 has the most error in the volume fraction field, but this error is reduced by more than a factor of two if the ACDI terms are active. Coralic & Colonius (2014) noted that adding a sharpening term to the phase field variable generally destroys conservation and causes improper final shock locations. However, since ACDI is in fully conservative form, all shock locations are accurate even though an active sharpening term is present. The sharpening term allows ACDI to keep the material interface thinner than WENO5 (the most dissipative scheme shown). Figure 2 also shows that adding the ACDI terms generally decreases the error in the other flow field variables as well — likely due to the sharper material interface. Overall, adding the ACDI terms to the ENO-type

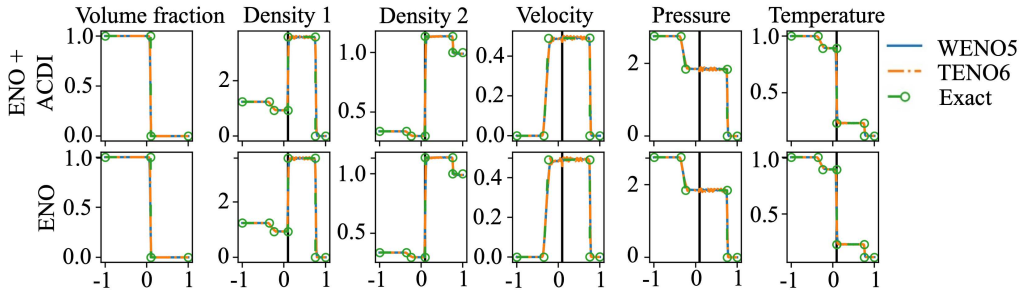

FIGURE 3. Plots of volume fraction, phase densities, velocity, pressure, and temperature for the gas–liquid Riemann problem at $t = 0.2$. The material interface location is marked in other flow fields with a black line.

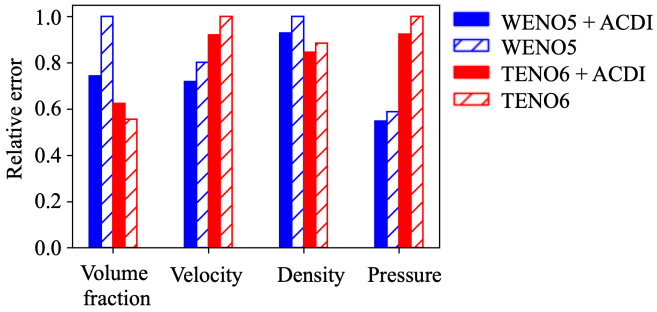

FIGURE 4. Relative error for the volume fraction, velocity, density, and pressure fields for each discretization scheme used to solve the gas–liquid Riemann problem.

schemes properly captures the shock discontinuity, provides a sharper material interface, and generally improves the accuracy of other flow variables.

3.1.2. *Gas-liquid shock tube*

Another shock tube test case is a gas-liquid problem first analyzed by Cocchi *et al.* (1996). The left state is highly compressed air, and the right state is water at atmospheric pressure. This one-dimensional case is a difficult numerical test and was formulated as a model problem for an underwater explosion. The same initial setup used in Coralic & Colonius (2014) is repeated here. The simulation uses 200 grid points with Dirichlet boundary conditions and an initial condition given by

$$(m_1, m_2, u, P, \phi_1) = \begin{cases} (1.241, 0.0, 0.0, 2.753, 1.0) & \text{if } -1 \leq x < 0.0, \\ (0.0, 0.991, 0.0, 0.0003059, 1.0) & \text{if } -0.8 \leq x \leq 1.0. \end{cases} \tag{3.2}$$

In Figure 3 the exact solution is plotted against both ENO-schemes with and without ACDI terms for the gas-liquid shock tube. All schemes match the shock locations, but also create visual oscillations around the material interface. This is a difficult test case for the four-equation model since the IEC is not discretely satisfied and is likely the cause of these oscillations. Even so, the results can be quantitatively compared to the exact solution.

Figure 4 shows the relative error for all schemes after solving the gas-liquid shock

tube problem. Adding ACDI to WENO5 sharpens the material interface (seen through the decrease in volume fraction error), but this is no longer true for TENO6. Given the initial condition of a coincident shock and material interface, the material interface is "self-sharpening" for some time. This allows TENO6 without the ACDI terms to have a sharper volume fraction profile. Though the interface is thicker for TENO6 + ACDI, the extra dissipation from the ACDI terms decreases the oscillations observed, which decreases the overall error for the other flow field variables. Overall, adding the ACDI terms improves the solution by lowering the error for most flow variables and still provides a relatively sharp material interface.

3.2. *Rayleigh–Taylor instability*

To illustrate the robustness of the ENO-type schemes, Rayleigh–Taylor instability simulations are carried out at low resolutions with $We = \infty$, $At = 0.667$, $\mu_1/\mu_2 = 10$, and a range of Reynolds numbers from $Re = 1.56 \times 10^2$ to $Re = 1.56 \times 10^5$. The domain is defined with an x-length of 1, a y-length of 3, and a uniform grid-size (Δ) of 1/64 in both directions. Periodic conditions are used for the x-boundaries and adiabatic walls for the y-boundaries. The perturbation in the solution was initialized using a profile for the volume fraction given by,

$$\phi_1 = 1/2 \left[1 + \tanh \left(\frac{y - 1.86 - 0.03 \cos(2\pi x)}{2\Delta} \right) \right]. \tag{3.3}$$

The solution was run until $t = 1.277$ with a CFL = 0.6. This simulation is repeated for a range of Reynolds numbers at the same grid resolution to show the weaknesses of WENO and TENO schemes for coarse grids. First, the interface shape and thickness with and without the ACDI terms are analyzed. Second, the ability of the ACDI terms improve the boundedness properties of ENO-type schemes bounded is shown. As a reference for how the ACDI terms resolve the solution without the ENO-like discretization, a sixth-order kinetic energy and entropy preserving (KEEP) skew-symmetric scheme is included. This is a high-order extension of the second-order formulation presented by Jain & Moin (2022).

3.2.1. *Interface shape and thickness*

Figure 5 shows how the different schemes compare for different Reynolds numbers. An important observation is that the symmetry of the solution is not captured by TENO6 unless ample resolution is provided in proportion to the Reynolds number. The lack of symmetry for TENO is generally caused by uncontrolled round-off errors and has been described in other works (Fleischmann *et al.* 2019). The effect of the ACDI terms on controlling the diffusion of the interface is apparent for both WENO5 and TENO6 at relatively low Reynolds number ($\sim 10^3$) and becomes dramatic at the largest Reynolds number ($\sim 10^5$). Visually, the diffusion of the material interface is manifested through the wispy structures and can be seen in all WENO5 and TENO6 solutions. These wispy structures represent mixing of the two phases, which is unphysical in an immiscible two-phase system. Often, for diffuse interface simulations, the volume fraction of 0.5 is used to represent the "sharp" cutoff between phases. For both WENO5 and TENO6 without ACDI, this is no longer applicable in the wispy regions. Overall, the mixing of immiscible phases is inevitable if WENO5 or TENO6 are used without interface regularization.

By contrast, adding the ACDI terms did an adequate job of keeping immiscible fluids immiscible and provided an interface with a finite and resolvable thickness. In all cases in

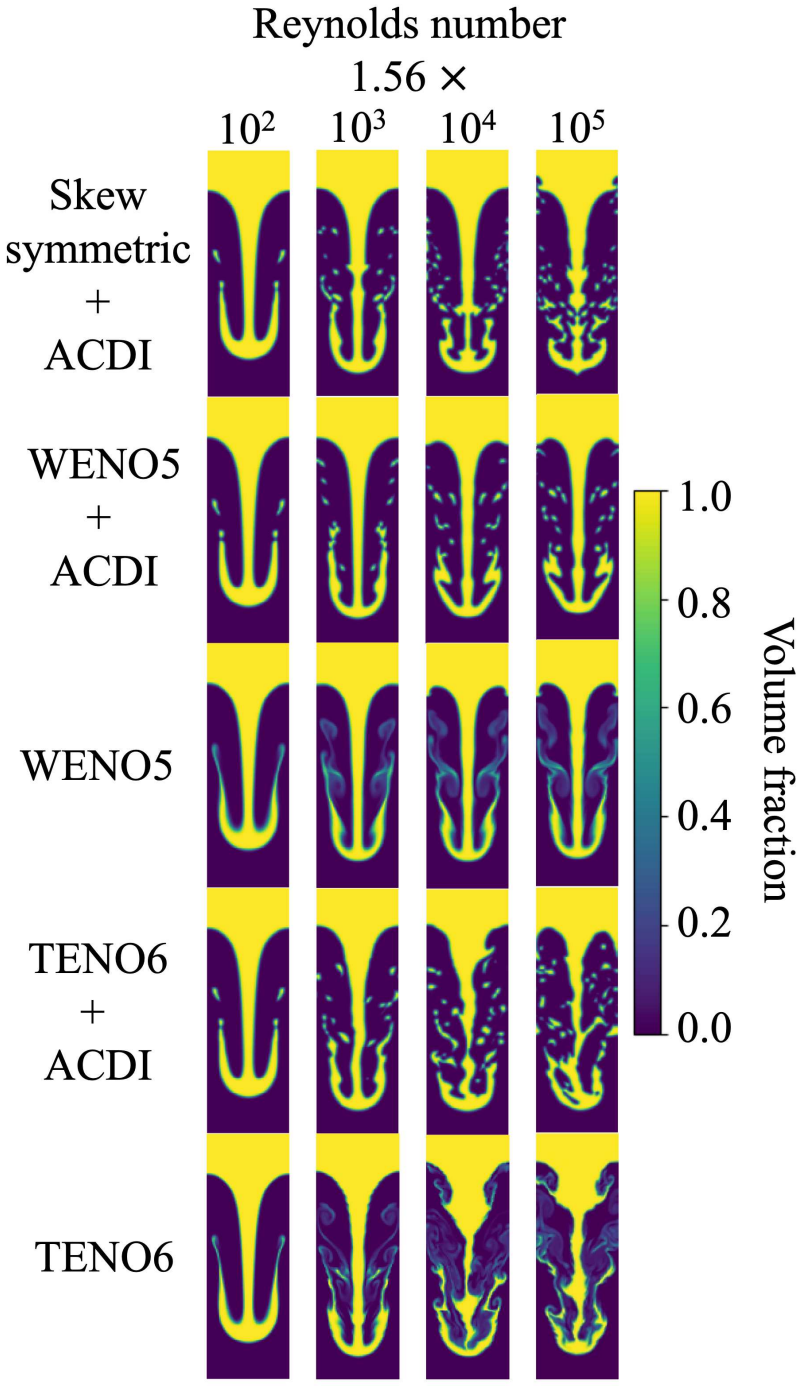

FIGURE 5. An array of Rayleigh-Taylor simulations for varying Re between 1.56×10^2 and 1.56×10^5 that highlight the differences in interface shape and thickness for each numerical scheme.

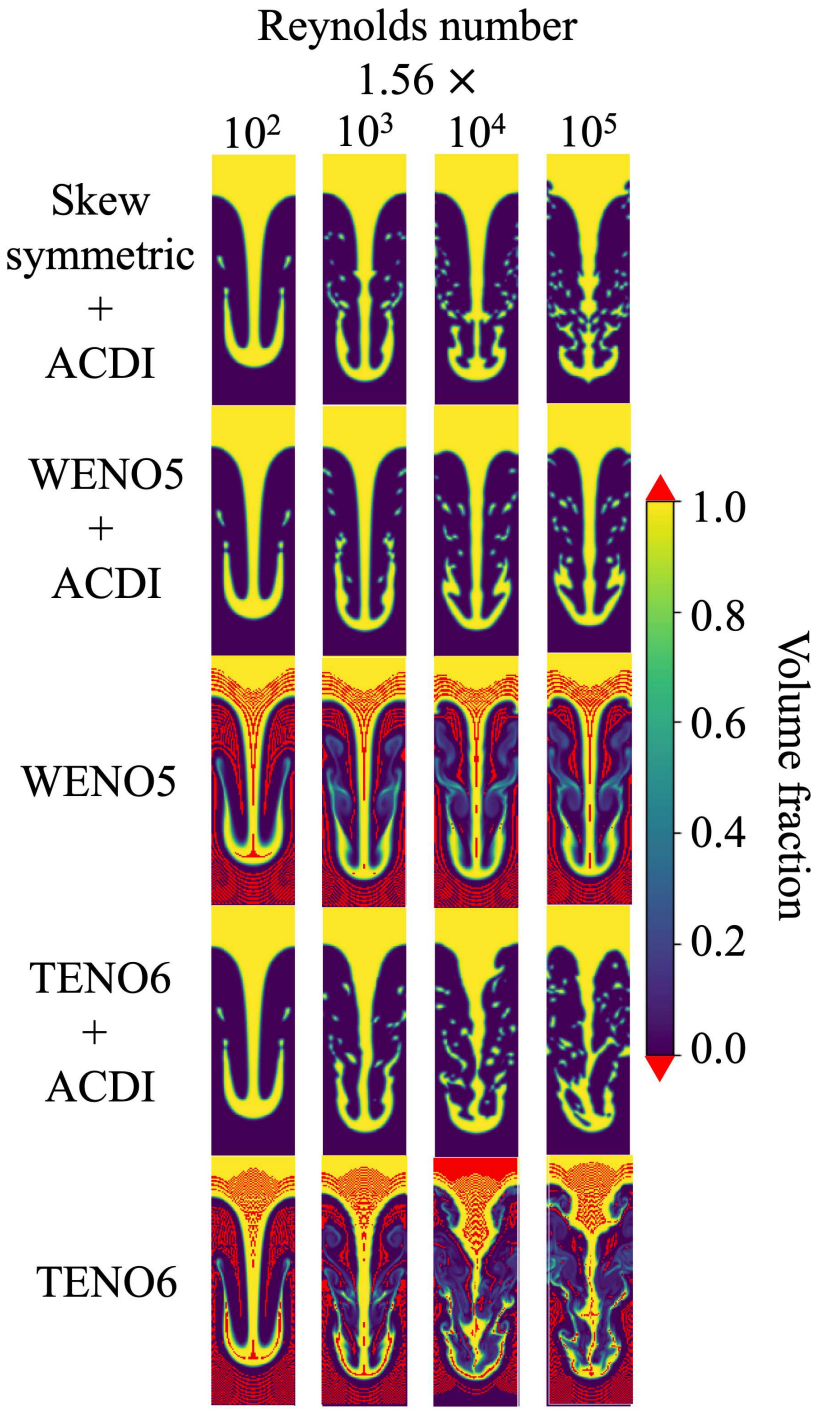

FIGURE 6. An array of Rayleigh-Taylor simulations for varying Re between 1.56×10^2 and 1.56×10^5 that highlight the computational cells that break the volume fraction boundedness requirement.

Figure 5, the phases stay immiscible and the phase field variable is able to visually indicate the current phase of the simulation cell. However, in order to keep the interface thickness finite in an under-resolved simulation, the ACDI terms cause a numerical breakup of the interface.

3.2.2. *Volume fraction boundedness*

Figure 6 shows the same Rayleigh–Taylor simulations as Figure 5, but highlights every cell that violates boundedness (volume fraction goes above 1.0 or below 0.0). Without adding the ACDI terms to the ENO-type schemes, many cells do not satisfy the boundedness requirement. The max boundedness error increases with Reynolds number and in some cases can cause simulations to crash due to highly unphysical (negative) mass fractions and densities polluting the speed of sound calculation and making it imaginary. In contrast, adding the ACDI terms provides results that are perfectly bounded for all snapshots shown, even up to the largest Reynolds number tested. This is a large improvement granted by adding the ACDI terms.

3.3. *Helium-air shock bubble interaction*

The final test case is a 2D shock-bubble interaction problem that combines shocks and interface deformations in one simulation. This test case has been studied extensively both computationally and experimentally and can act as a validation of the numerical method. The problem consists of a Mach 1.22 shock wave traveling from right to left in air at atmospheric pressure toward a helium bubble. The setup is very similar to that used by Jain (2021). The domain is defined with a uniform grid-size $\Delta = 0.01$ with x-length = 6 and y-length = 1. A non-reflective boundary condition is located at x = 6, an adiabatic wall at x = 0, and periodic boundaries at y = 0 and y = 1. The material properties for air are $\gamma_1 = 1.4$ and $\rho_1 = 1.0$. The material properties for helium are $\gamma_2 = 1.67$ and $\rho_2 = 0.138$. The initial condition for this problem is a drop of helium with radius 25/89 centered at y=1/2 and x=4 surrounded by air. This is given by

$$\begin{gathered} f_s = \frac{1}{2}\operatorname{erfc}\Big(\frac{x-5}{2\Delta}\Big), \\ u = u^{(2)} f_s + u^{(1)}(1-f_s), \quad v = 0, \quad P = P^{(2)} f_s + P^{(1)}(1-f_s), \\ \phi_1 = \frac{1}{2}\operatorname{erfc}\Big[\frac{625/7921 - (x-4)^2 - (y-1/2)^2}{\Delta}\Big], \quad \text{and} \\ \rho = (\phi_1\rho_1 + (1-\phi_1)\rho_2)\Big[\frac{\rho^{(2)}}{\rho^{(1)}} f_s + (1-f_s)\Big], \end{gathered} \tag{3.4}$$

where the post/pre shock conditions are, $u^{(1)} = 0.39473$, $u^{(2)} = 0.0$, $P^{(1)} = 1.5698$, $P^{(2)} = 1$, $\rho^{(1)} = 1.3763$, and $\rho^{(2)} = 1.0$. The problem was simulated using a constant $\Delta t = 0.001$.

Figure 7 shows qualitative results similar to those from the Rayleigh–Taylor simulations in Section 3.2. WENO5 and TENO6 continually diffuse the material interface throughout time and result in unphysical mixing of immiscible fluids. If the ACDI terms are active, the locations where the physical interface is thinner than the grid scale go through numerically induced breakup to ensure the material interface is resolved by the grid.

Lastly, Figure 8 shows all locations where volume fraction boundedness is no longer satisfied. As expected, WENO5 and TENO6 both break the boundedness requirement in many locations. Adding the ACDI terms to the WENO5 simulation kept the solution bounded, but the ACDI terms did not keep the TENO6 simulation perfectly bounded.

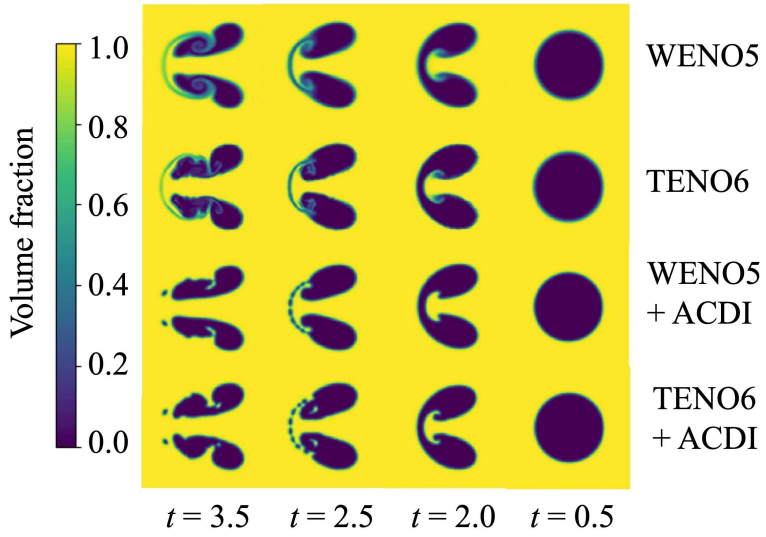

FIGURE 7. Four snapshots of a shock-bubble interaction that highlight the differences in interface shape and thickness for each numerical scheme.

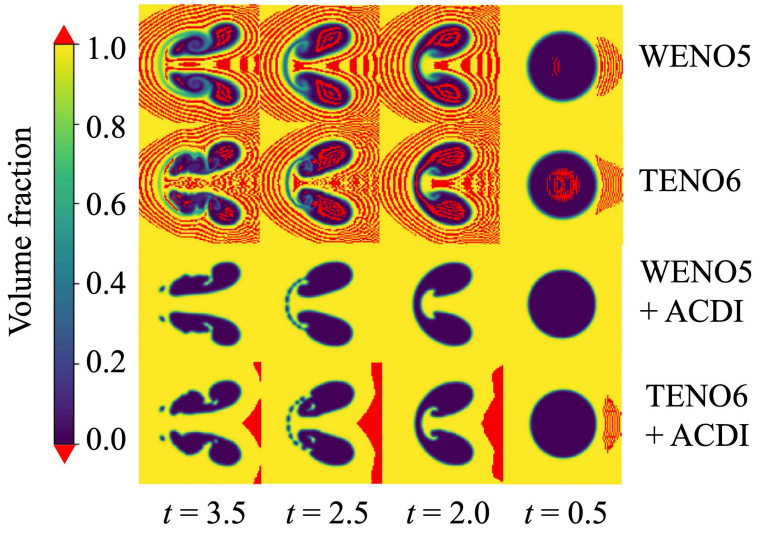

FIGURE 8. Four snapshots of a shock-bubble interaction that highlight the computational cells that break the volume fraction boundedness requirement.

This should not be entirely surprising because the boundedness criteria is strictly satisfied only for second-order centered-difference schemes. To quantitatively compare these results, the maximum volume fraction error for TENO6 with and without ACDI is shown in Table 1. Importantly, the behavior of the boundedness error is completely different between TENO6 and TENO6 + ACDI. Adding the ACDI terms to the ENO-type scheme decreases the boundedness error with time and approaches machine precision. By contrast, using TENO6 without the ACDI terms results in amplified boundedness error

	$t = 0.5$	$t = 2.0$	$t = 2.5$	$t = 3.5$
TENO6	2.2×10^{-5}	8.1×10^{-3}	1.1×10^{-2}	1.2×10^{-1}
TENO6 + ACDI	7.5×10^{-7}	1.1×10^{-11}	6.8×10^{-12}	3.5×10^{-12}

TABLE 1. Shock-bubble boundedness errors for TENO6 and TENO6 + ACDI.

throughout time and approaches becoming an O(1) error for an O(1) quantity, making the method unusable for longer simulations.

4. Conclusions

In this work, two commonly used ENO-like discretization schemes were evaluated for their applicability to simulation of compressible two-phase flows using a diffuse interface method. WENO and TENO have been previously shown to be robust for shocks and other flow discontinuities. In this work, in the framework of the four-equation two-phase model in conjunction with the stiffened gas equation of state, the performance of WENO and TENO schemes for simulations of compressible two-phase flows was evaluated. A particularly unique aspect of this work is the assessment of the WENO and TENO schemes coupled with recently developed accurate conservative diffuse interface regularization terms. Using multiple 1D and 2D test cases, it was shown that coupling WENO or TENO with interface regularization terms provides improvements over using these diffuse interface methods separately. Using ENO-type schemes with the ACDI terms provides a simulation framework that creates resolvable but finite thickness material interfaces, has drastically improved robustness for achieving bounded volume fractions, and captures different types of discontinuities without parameter tuning.

Acknowledgments

This investigation was funded by the US Department of Energy's National Nuclear Security Administration via the PSAAP-III Center at Stanford, Award No. DE-NA0003968. Authors are thankful for the comments from Reed Brown who helped improve this article with his thoughtful review. H. Collis is also thankful for Dr. Mario Di Renzo, Dr. Jonathan Wang, and Chris Williams, for providing invaluable expertise on ENO-schemes and their efficient implementation in HTR.

REFERENCES

BAER, M. R. & NUNZIATO, J. W. 1986 A two-phase mixture theory for the deflagration-to-detonation transition (DDT) in reactive granular materials. *Int. J. Multiphas. Flow* **12**, 861–889.

CHIU, P.-H. & LIN, Y.-T. 2011 A conservative phase field method for solving incompressible two-phase flows. *J. Comput. Phys.* **230**, 185–204.

Cocchi, J., Saurel, R. & Loraud, J. 1996 Treatment of interface problems with Godunov-type schemes. *Shock Waves* **5**, 347–357.

Cook, A. W. 2007 Artificial fluid properties for large-eddy simulation of compressible turbulent mixing. *Phys. Fluids* **19**, 055103.

Cook, A. W. & Cabot, W. H. 2005 Hyperviscosity for shock-turbulence interactions. *J. Comput. Phys.* **203**, 379–385.

Coralic, V. & Colonius, T. 2014 Finite-volume WENO scheme for viscous compressible multicomponent flows. *J. Comput. Phys.* **274**, 95–121.

Di Renzo, M., Fu, L. & Urzay, J. 2020 HTR solver: an open-source exascale-oriented task-based multi-gpu high-order code for hypersonic aerothermodynamics. *Comput. Phys. Commun.* **255**, 107262.

Flåtten, T., Morin, A. & Munkejord, T. 2011 On solutions to equilibrium problems for systems of stiffened gases. *SIAM J. Appl. Math.* **71**, 41–67.

Fleischmann, N., Adami, S. & Adams, N. A. 2019 Numerical symmetry-preserving techniques for low-dissipation shock-capturing schemes. *Comput. Fluids* **189**, 94–107.

Fu, L. 2019 A low-dissipation finite-volume method based on a new TENO shock-capturing scheme. *Comput. Phys. Commun.* **235**, 25–39.

Fu, L., Hu, X. Y. & Adams, N. A. 2016 A family of high-order targeted ENO schemes for compressible-fluid simulations. *J. Comput. Phys.* **305**, 333–359.

Harten, A., Engquist, B., Osher, S. & Chakravarthy, S. R. 1987 Uniformly high order accurate essentially non-oscillatory schemes, III. *J. Comput. Phys.* **71**, 231–303.

Jain, S. S. 2021 A novel diffuse-interface model and numerical methods for compressible turbulent two-phase flows and scalar transport. PhD thesis, *Stanford University*.

Jain, S. S. 2022 Accurate conservative phase-field method for simulation of two-phase flows. *J. Comput. Phys.* **469**, 111529.

Jain, S. S., Adler, M. C., West, J. R., Mani, A., Moin, P. & Lele, S. K. 2023 Assessment of diffuse-interface methods for compressible multiphase fluid flows and elastic-plastic deformation in solids. *J. Comput. Phys.*, 111866

Jain, S. S., Mani, A. & Moin, P. 2020 A conservative diffuse-interface method for compressible two-phase flows. *J. Comput. Phys.* **418**, 109606.

Jain, S. S. & Moin, P. 2021 Stable, entropy-consistent, and localized artificial-viscosity method for capturing shocks and contact discontinuities. *Annual Research Briefs*, Center for Turbulence Research, Stanford University. pp. 169–181.

Jain, S. S. & Moin, P. 2022 A kinetic energy–and entropy-preserving scheme for compressible two-phase flows. *J. Comput. Phys.* **464**, 111307.

Jiang, G. S. & Shu, C. W. 1996 Efficient implementation of weighted ENO schemes. *J. Comput. Phys.* **126**, 202–228.

Johnsen, E. & Colonius, T. 2006 Implementation of WENO schemes in compressible multicomponent flow problems. *J. Comput. Phys.* **219**, 715–732.

Johnsen, E. & Colonius, T. 2009 Numerical simulations of non-spherical bubble collapse. *J. Fluid. Mech.* **629**, 231–262.

Johnsen, E. & Ham, F. 2012 Preventing numerical errors generated by interface-capturing schemes in compressible multi-material flows. *J. Comput. Phys.* **231**, 5705–5717.

Kawai, S. & Lele, S. K. 2008 Localized artificial diffusivity scheme for discontinuity capturing on curvilinear meshes. *J. Comput. Phys.* **227**, 9498–9526.

Liu, T., Khoo, B. & Yeo, K. 2003 Ghost fluid method for strong shock impacting on material interface. *J. Comput. Phys.* **190** (2), 651–681.

Liu, X. D. 1994 Weighted essentially non-oscillatory schemes. *J. Comput. Phys.* **115**, 200–212.

Mani, A., Larsson, J. & Moin, P. 2009 Suitability of artificial bulk viscosity for large-eddy simulation of turbulent flows with shocks. *J. Comput. Phys.* **228**, 7368–7374.

Mirjalili, S., Ivey, C. B. & Mani, A. 2020 A conservative diffuse interface method for two-phase flows with provable boundedness properties. *J. Comput. Phys.* **401**, 109006.

Mirjalili, S., Taverniers, S., Collis, H., Behandish, M. & Mani, A. 2021 A localized artificial diffusivity approach inspired by TVD schemes and its consistent application to compressible flows. *Annual Research Briefs*, Center for Turbulence Research, Stanford University, pp. 169–181.

Movahed, P. & Johnsen, E. 2013 A solution-adaptive method for efficient compressible multifluid simulations, with application to the Richtmyer–Meshkov instability. *J. Comput. Phys.* **239**, 166–186.

Pirozzoli, S. 2011 Numerical methods for high-speed flows. *Annu. Rev. Fluid Mech.* **43**, 163–194.

San, O. & Kara, K. 2014 Numerical assessments of high-order accurate shock capturing schemes: Kelvin-Helmholtz type vortical structures in high-resolutions. *Comput. Fluids* **89**, 254–276.

Saurel, R. & Pantano, C. 2018 Diffuse-interface capturing methods for compressible two-phase flows. *Annu. Rev. Fluid Mech.* **50**.

Shu, C. W. & Osher, S. 1988 Efficient implementation of essentially non-oscillatory shock-capturing schemes. *J. Comput. Phys.* **77**, 439–471.

Shu, C. W. & Osher, S. 1989 Efficient implementation of essentially non-oscillatory shock-capturing schemes, II. *J. Comput. Phys.* **83**, 32–78.

Shukla, R. K., Pantano, C. & Freund, J. B. 2010 An interface capturing method for the simulation of multi-phase compressible flows. *J. Comput. Phys.* **229**, 7411–7439.

Subramaniam, A., Ghaisas, N. S. & Lele, S. K. 2018 High-order eulerian simulations of multimaterial elastic–plastic flow. *J. Fluids ENG-T ASME Eng.* **140**, 050904.

Tiwari, A., Freund, J. B. & Pantano, C. 2013 A diffuse interface model with immiscibility preservation. *J. Comput. Phys.* **252**, 290–309.

Wong, M. L., Angel, J. B., Barad, M. F. & Kiris, C. C. 2021 A positivity-preserving high-order weighted compact nonlinear scheme for compressible gas-liquid flows. *J. Comput. Phys.* **444**, 110569.